analytical chemistry

Article

pubs.acs.org/ac

Surface-Induced Dissociation of Ion Mobility-Separated Noncovalent Complexes in a Quadrupole/Time-of-Flight Mass Spectrometer

Mowei Zhou, Chengsi Huang, and Vicki H. Wysocki*

Department of Chemistry and Biochemistry, University of Arizona, 1306 E. University Boulevard, PO Box 210041, Tucson, Arizona 85721-0041, United States

ABSTRACT: A custom in-line surface-induced dissociation (SID) device has been incorporated into a commercial ion mobility quadrupole/time-of-flight mass spectrometer in order to provide an alternative and potentially more informative activation method than the commonly used collision-induced dissociation (CID). Complicated sample mixtures can be fractionated by ion mobility (IM) and then dissociated by CID or SID for further structural analysis. Interpretation of SID spectra for cesium iodide clusters was greatly simplified with IM prior to dissociation because products originating from different precursors and overlapping in m/z but separated in drift time can be examined individually. Multiple conformations of two protein complexes, source-activated transthyretin tetramer and nativelike serum amyloid P decamer, were separated in ion mobility and subjected to CID and SID. CID spectra of the mobility separated conformations are similar. However, drastic differences can be observed for SID spectra of different conformations, implying different structures in the gas phase. This work highlights the potential of utilizing IM-SID to study quaternary structures of protein complexes and provides information that is complementary to our recently reported SID-IM approach.

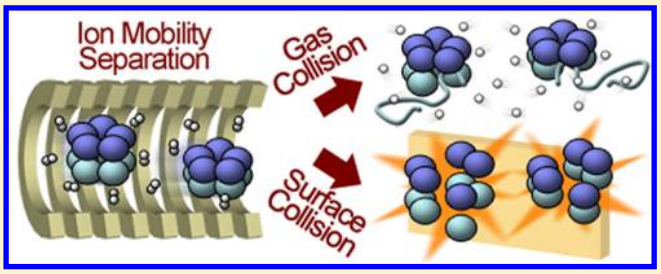

The introduction of native mass spectrometry,[1−4] in which the noncovalent interactions stabilizing protein complexes or other supramolecular systems can be maintained under gentle electrospray conditions, has boosted the application of mass spectrometry to structural biology. The stoichiometry of protein complexes can be determined from a mass measurement with very low sample consumption and simple sample preparation because of the sensitivity and short analysis time of mass spectrometry. Ideally, tandem mass spectrometry (MS/MS) experiments can be employed to determine the arrangement of subunits in the complexes. Collision-induced dissociation (CID) is a widely available MS/MS activation method that involves activation of the precursor upon collision with neutral gas atoms or molecules. Alternatively, activation in MS/MS can be achieved by the impact of the precursor on a surface target. In typical low energy (eV) CID experiments,[5,6] the kinetic energy of the precursor is converted to its internal energy through multiple collision events with neutral gas atoms/molecules, while an approximately single-step energy transfer is likely the mechanism for surface-induced dissociation (SID) at acceleration voltages comparable to those used in CID.[7] Due to the stepwise nature of energy deposition in low energy CID, the dissociation pathways with lower activation barriers usually lead to the dominant ions detected in the experiment. In contrast, the larger amount of energy deposited into the precursor within a single step by SID makes pathways with higher energy barriers available in competition with the slower, lower barrier processes. Furthermore, SID has been shown to have efficiency higher than that of CID in transferring the kinetic energy to the internal energy of the ions, because of the much larger relative effective mass of the surface to the precursor compared with the mass of small gaseous collision targets relative to the precursor.[6]

Our research group has shown in the past that SID results in significantly different dissociation spectra from CID for noncovalent complexes at comparable laboratory frame acceleration voltages.[7,8] The protein complexes tend to dissociate in a more charge-symmetric way in SID, with each product carrying a number of charges that is proportional to its mass.[7] However, CID frequently dissociates the complex in a highly asymmetrical fashion, with low mass products retaining a high percentage of the charge from the precursor. A plausible mechanism for asymmetric dissociation of protein complexes in CID, supported by both experimental and theoretical studies from several groups,[9−15] is the gradual unfolding of a monomer subunit followed by the ejection of the highly charged monomer. The lower charge states, as well as the compactness of the SID products revealed by our ion mobility measurements with a pentameric protein complex,[16] suggest that certain complexes can dissociate into noncovalent subunits by SID without significant unfolding. It is important to realize that more representative quaternary structures of the native protein complexes can be determined from the dissociation information if the protein complexes have not undergone significant conformational change during the activation process. Although one may expect nonergodic activation methods such as electron

Received: March 22, 2012
Accepted: June 8, 2012
Published: June 8, 2012

   dx.doi.org/10.1021/ac300810u | *Anal. Chem.* 2012, 84, 6016−6023

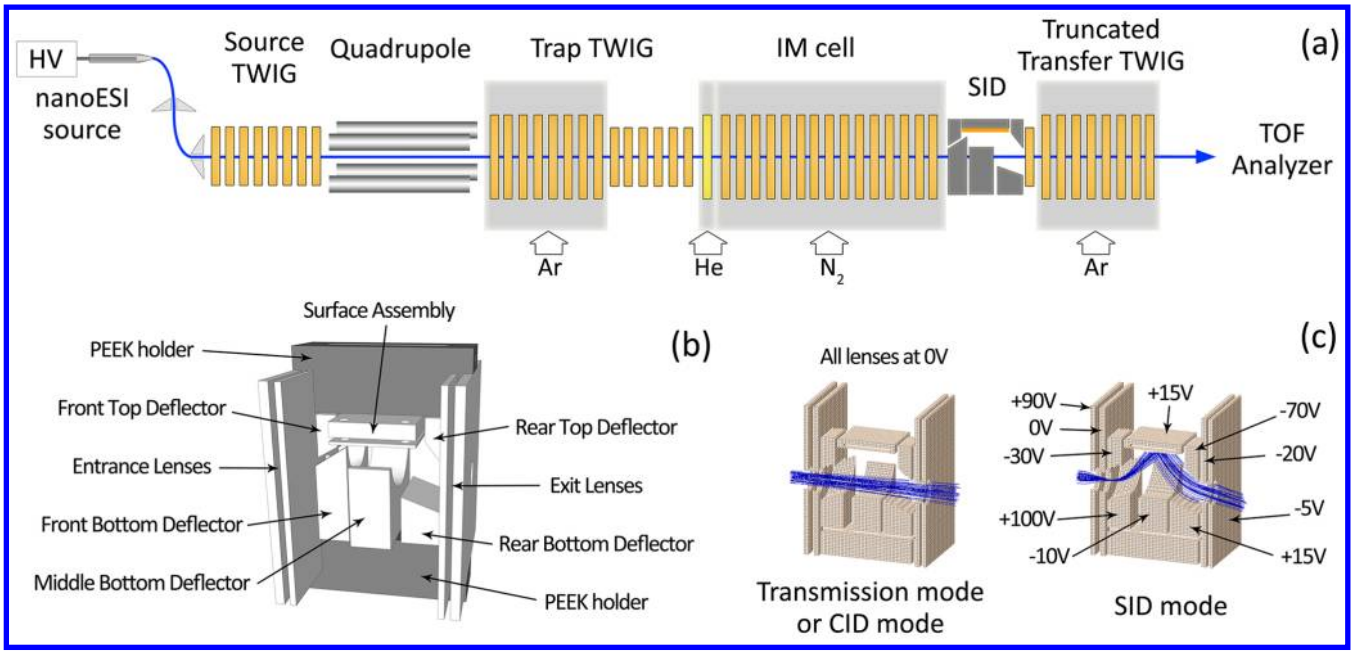

Figure 1. (a) Schematic view of the modified Waters Synapt G2 with SID capability. Dimensions of the ion optics are not drawn to scale. The lighter gray shaded regions are enclosed cells which are filled with gas as indicated by the arrows below them. The exposed region of original transfer TWIG was truncated to accommodate the SID device. (b) 3D perspective view of the SID device assembly. (c) Cutaway views of SIMION simulation showing the ion path in transmission/CID mode and SID mode. Typical voltages on the SID lenses relative to the potential on the downstream transfer TWIG are labeled. The optimal voltages in SID experiments vary at different collision energies.

capture dissociation (ECD) and electron transfer dissociation (ETD) to cause dissociation of protein complexes without conformational disruption, experiments from Zhang et al.[17] show covalent peptide backbone fragmentations of several protein complexes in ECD. Their data provide structural insights into flexible regions of the complexes, but information of protein quaternary structures is very limited due to lack of subunit ejection. Recent SID work from our group[18] has shown substructure characterization for a heterohexameric protein complex, toyocamycin nitrile hydratase, which dissociates into two $\alpha\beta\gamma$ trimers, suggesting that the native structure is a dimer of trimers, in agreement with another known nitrile hydratase. The robustness of MS/MS analysis in providing topology information of protein complexes makes it appealing for characterization of proteins that are difficult to crystallize and/or purify for X-ray crystallography and nuclear magnetic resonance, respectively.

The combination of ion mobility (IM) and mass spectrometry has gained popularity for structure analysis of biological complexes, including peptide oligomers[19,20] and protein assemblies.[21−24] With IM, ions are separated in the gas phase under the influence of a bath gas and an electric field based on their difference in shape. Complicated samples containing species overlapping in mass-to-charge (m/z) that cannot be resolved by mass spectrometry alone, such as isomers, and different charge states of different oligomers and conformers, can be separated by IM for subsequent identification with intact mass measurements or MS/MS. Liquid phase separation techniques such as size exclusion chromatography (SEC)[25] and flow field-flow fractionation (F4)[26] are indispensable to separation of intact proteins and protein complexes. The conditions of SEC might not be gentle enough to preserve the native conformation of fragile noncovalent complexes due to high salt concentration, and mechanical stress from interaction between analytes and stationary phases.[26] F4, where separation relies on diffusion coefficients of the analytes, has been developed as an alternative technique without a stationary phase and shows promising results for protein fractionation.[26] These liquid phase techniques usually serve as prefractionation steps in sample preparation and require a few minutes or even longer. On the other hand, IM can be directly interfaced to MS, either prior to or after m/z selection of a precursor, and the time scale of IM is usually in the millisecond regime, which makes separation and analysis of short-lived structures possible. Unfolding intermediates of several protein complexes have been studied using IM-MS, providing insights on stability of the complexes in the gas phase.[27−30]

In the work reported here a custom SID device was designed and installed into a modified quadrupole-IM-time-of-flight instrument. The inserted SID device, which is after the IM cell in the current setup, enables post-IM SID on m/z- and shape-separated precursors in addition to the post-IM CID available in the original instrument. Cesium iodide clusters with overlapping m/z, and protein complexes with multiple conformations, were studied to illustrate the advantage of the IM-SID modification over conventional quadrupole-time-of-flight mass spectrometers; unique information on the structures of the complexes is provided.

EXPERIMENTAL SECTION

Modification of the Commercial Instrument. A commercial quadrupole-IM-time-of-flight (Q-IM-TOF) mass spectrometer (Synapt G2, Waters Corporation, Manchester, United Kingdom) was modified to incorporate an in-line SID device. A schematic view of the modified instrument is shown in Figure 1a. Further descriptions of the commercial instrument can be found elsewhere.[31,32] The T-wave ion guide (TWIG) in the transfer region was truncated by 3 cm, without damaging critical electrical parts to accommodate our custom-made SID

dx.doi.org/10.1021/ac300810u | Anal. Chem. 2012, 84, 6016−6023

device (Figure 1a). The design of SID was adapted from the previous generation SID device used in our group[33] with some changes to the geometry and dimensions. The schematic view of the current SID design is illustrated in Figure 1b. Simulations in SIMION 7.0 (Idaho National Engineering and Environmental Laboratory, Idaho Falls, ID) showed that the new device design functions similarly to the previous design despite the smaller dimension. The SID lenses are stainless steel and are assembled on PEEK (McMaster-Carr, Cleveland, OH) holders. The setup is mounted on an aluminum holder and positioned between the IM cell and the truncated transfer TWIG. Each SID lens (10 total) is electrically connected through a spare connection port on the side of the TWIG chamber to an individual channel of two external DC power supplies (each has nine channels; Spectrum Solutions Inc., Russellton, PA) via a 12-pin connector (Molex, Lisle, IL). All the lenses and holders were fabricated by the University Machine Shop and the Chemistry and Biochemistry Department Machine Shop at the University of Arizona.

Materials and Methods. Glass capillaries for nanoelectrospray (nanoESI) were pulled in-house (Sutter Instruments, P-97 micropipet puller, Novato, CA). A custom static sprayer which consumes much less sample was used to replace the original nanoESI source sprayer of the instrument. A platinum wire on the static sprayer was inserted into the capillary to apply high voltage (0.9−1.5 kV) for nanoESI, and the sample solution was loaded into the capillary. No source gas was applied. The backing pressure in the source was adjusted to 5−6 mbar for optimization of signal for noncovalent complexes. The sample cone voltage typically used is 15−50 V. The SID surface used in the experiment is a glass surface coated with 10 Å of titanium and 1000 Å of gold (Evaporated Metal Films Corp., Ithaca, NY). Prior to use, the surface is further chemically modified with 2-(perfluorodecyl)ethanethiol following a protocol described elsewhere.[33]

Peptides with reverse sequences (SDGRG and GRGDS) were kindly supplied by Waters Corporation (ERA, Arvada, CO). Cesium iodide was purchased from Sigma-Aldrich (99.999%, Allentown, PA) and used without further purification. The CsI and reverse peptides were dissolved in acetonitrile:water:formic acid (50:50:0.1) solution for nanoESI. Lyophilized powder of human transthyretin (Sigma-Aldrich, Saint Louis, MO) and human serum amyloid P (CalBiochem, San Diego, CA) was dissolved in water and exchanged into 100 mM and 200 mM pH 7 ammonium acetate buffer, respectively, with size exclusion chromatography spin columns (BioRad, Hercules, CA) before analysis. The concentrations of proteins used are 25 μM for transthyretin tetramer (56k Da) and 100 μM/monomer for serum amyloid P (23.5 kDa per monomer). The source and bias voltages from the instrument tune page were optimized to allow a good transmission without significant activation for each precursor. Gas pressure and T-wave parameters were tuned for each sample. For peptide samples, the conditions were as follows: trap gas 2.5 mL/min, helium gas 180 mL/min, nitrogen 90 mL/min, IMS wave height 18 V, IMS wave velocity 320 m/s. For cesium iodide and protein samples, the conditions used were as follows: trap gas 4−6 mL/min, helium gas 120−160 mL/min, nitrogen 60−80 mL/min, IMS wave height 12−18 V, IMS wave velocity 180−250 m/s. All mass spectra were processed with MassLynx v4.1 and DriftScope v2.1 (Waters Corporation, Manchester, United Kingdom).

Operation of the Modified Instrument. When operating in IM-TOF mode, the ions are trapped in the trap TWIG and released in pulses into a pressurized IM cell where the ions undergo separation based on their charge, size, and shape. The helium cell in front of the IM cell reduces the kinetic energy of the ions, thus improving the subsequent IM resolution.[31] The ions exiting the IM cell after separation will either be transmitted to the TOF analyzer or undergo MS/MS in the transfer region before entering the TOF. Shape-"selected" activation is realized through data processing by extracting the MS/MS spectra from precursors that are separated in drift time.

For CID experiments, the voltages on the SID device are set for fly-through transmission of the ions (Figure 1c, left). All the IM-CID experiments in this work were performed in the transfer TWIG by accelerating the ions exiting the IM cell before they entered the transfer TWIG region. In SID experiments, the potential on the front bottom deflector was raised to steer the ions onto the surface (Figure 1c, right). Other lenses were tuned for maximum transmission as indicated by the ion current at the detector. SID acceleration voltage is defined by the potential difference between the IM cell exit and the surface. This acceleration voltage does not directly reflect the effective SID collision energy because of the collision geometry (incident angle is about 45°) and possible loss of kinetic energy from collision with background gas before surface impact. Additionally, accurate determination of effective collision energies is complicated by the heterogeneity of the energies within large complexes. We do not intend to make a quantitative comparison between CID and SID collision energies. The acceleration voltages listed in the following discussions serve as qualitative estimates of the magnitude of collision under the accessible voltages of the instrument. The DC potential downstream of the surface, on the transfer TWIG, was held 10−20 V lower than that of the surface to provide sufficient acceleration of the SID product ions off the surface. Many factors including pressure, electrical lens aperture, and kinetic energies of the ions affect transmission. Furthermore, SID products are usually in an m/z region larger than that of CID products, where the instrument has intrinsically lower sensitivity. At this point, SID still has recovery lower than that of CID even after careful optimization of experimental conditions, but the results presented here, which show high signal-to-noise ratio SID spectra comparable to those from CID, are representative of the qualitative differences between the two activation methods. For initial instrument testing, a peptide mixture containing GRGDS and SDGRG (m/z = 246, doubly charged), a model system originally developed by Hill et al.,[34] was separated in drift time with a resolution of 1.0 ($t/\Delta t$) and fragmented by CID or SID (data not shown). The reverse peptides are fragile upon fragmentation; thus, both CID and SID are able to access all the fragmentation pathways available in this energy regime, with some differences noted in the ratios of product ions.

RESULTS AND DISCUSSION

Complexity of MS/MS Spectra of Cesium Iodide Clusters Is Greatly Reduced after IM Separation. Alkali halide cluster ions have been used as a model system to study fundamental physical properties of clusters.[35,36] Cesium iodide clusters $Cs_x(CsI)_y^{x+}$ can be readily formed by electrospray and are commonly used as a calibration standard in mass spectrometry. Our group has previously reported MS/MS of small CsI clusters in a Q/TOF instrument without mobility

dx.doi.org/10.1021/ac300810u | Anal. Chem. 2012, 84, 6016−6023

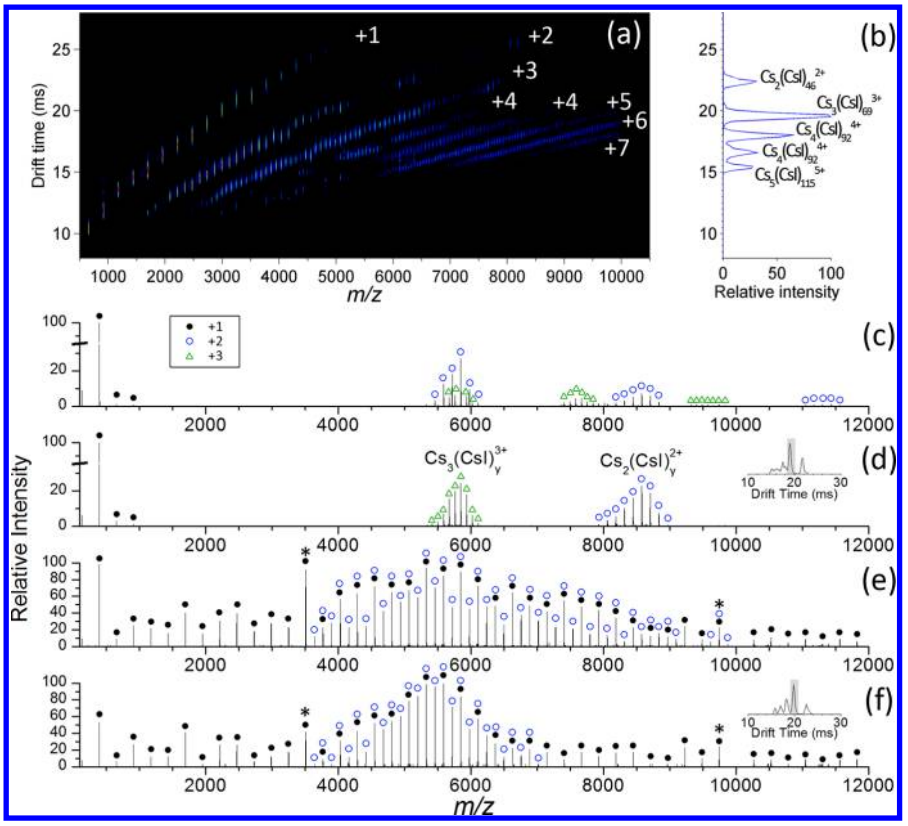

Figure 2. (a) IM-MS spectrum of CsI clusters. The brightness of the spots in the spectrum indicates the intensity of the species. (b) Drift time distribution of m/z 6108, which consists of overlapping multiply charged ions. (c) Convoluted CID spectrum at 65 V of all the ions $Cs_x(CsI)_{23x}^{x+}$ overlapping at m/z 6108.5. (d) Extracted CID spectrum of $Cs_3(CsI)_{69}^{3+}$ at 65 V. The inset shows the drift time distribution of CID products, and the shaded peak is the one whose spectrum is extracted here. (e) Convoluted SID spectrum at 65 V of all the ions $Cs_x(CsI)_{23x}^{x+}$ overlapping at m/z 6108.5. (f) Extracted SID spectrum at 65 V of $Cs_3(CsI)_{69}^{3+}$. The inset is the drift time distribution of all SID products from the multiply charged species, and the shaded peak corresponds to $Cs_3(CsI)_{69}^{3+}$. The asterisk-labeled peaks correspond to magic number clusters.

separaration of overlapping charge and oligomeric states.[8] There are some differences between CID and SID for small size clusters, but the differences are much more pronounced for medium and large size clusters. The dominant dissociation pathway of large CsI cluster ions in CID is the neutral loss of small numbers of $(CsI)_n$ from the original cluster, while SID cleaves the cluster in a more symmetric way, with charge separation among the products. However, the MS/MS spectra may be convoluted spectra with products from different multiply charged precursors overlapping in m/z, which complicates data interpretation. Here we present an example showing the mobility separation of $Cs_n(CsI)_{23n}^{n+}$, n = 2−5, and subsequent MS/MS in our modified instrument.

The IM-MS spectrum of CsI cluster ions is shown in Figure 2a. The presence of multiply charged clusters $Cs_x(CsI)_n^{x+}$ (x = 1−7) can be readily identified. Cluster ions with increasing "n" value at each charge state occupy an individual mobility space in the two-dimensional spectrum as indicated by the streaks with different slopes. The species with m/z 6108.5 was selected in the quadrupole, and the drift time distribution is shown in Figure 2b. With the information from the full MS spectrum (Figure 2a), the five major ion packets separated in drift time at m/z 6108.5 were identified to be overlapping $Cs_n(CsI)_{23n}^{n+}$ cluster ions with different charge states (n = 2−5). One interesting feature in the spectrum is that $Cs_4(CsI)_y^{4+}$ ions exhibited two distinct conformations (see the two streaks corresponding to the quadruply charged species in Figure 2a). The origin of these two conformations is beyond the scope of this work and is currently unclear. To demonstrate the IM-MS/MS capability of our modified instrument, multiply charged cluster ions which overlapped at m/z 6108.5 were separated in the IM cell and then subjected to CID or SID activation in the transfer TWIG region with an acceleration voltage of 65 V. Convoluted CID and SID spectra of all the species with various charge states are shown in Figure 2c,e, respectively. Without IM separation, interpretation of the MS/MS spectra would be difficult because products from multiple precursors (e.g., $Cs_2(CsI)_{46}^{2+}$, $Cs_3(CsI)_{69}^{3+}$, $Cs_4(CsI)_{92}^{4+}$) are convoluted in a single spectrum. Extracted CID and SID spectra for $Cs_3(CsI)_{69}^{3+}$ are listed in Figure 2d,f as representative examples.

Besides the dominant peak of Cs_2I^+ at m/z 392.7, the extracted CID spectrum of $Cs_3(CsI)_{69}^{3+}$, showed two groups of product ions at m/z around 5848.7 and 8576.4. The group of peaks around m/z 5848.7 is determined to be $Cs_3(CsI)_y^{3+}$ (y = 61−69) which correspond to neutral loss of 1 to 8 CsI (y = 61−68) from the precursor and the intact precursor (y = 69). The other group around m/z 8576.4 can be identified as $Cs_2(CsI)_y^{2+}$ (y = 60−66), which possibly came from the loss of Cs^+ from $Cs_3(CsI)_{69}^{3+}$ along with neutral loss of 3 to 9 CsI from the charge reduced ion. The dissociation pattern is consistent with previous studies from our group and suggests that energy deposition in CID is realized in a stepwise manner which leads to stripping of small subunits from the original cluster ion.

In contrast to the dominant neutral loss pathway in CID, the $Cs_3(CsI)_{69}^{3+}$ precursor cleaved into $Cs_2(CsI)_y^{2+}$ (y = 31−51) in

dx.doi.org/10.1021/ac300810u | Anal. Chem. 2012, 84, 6016−6023

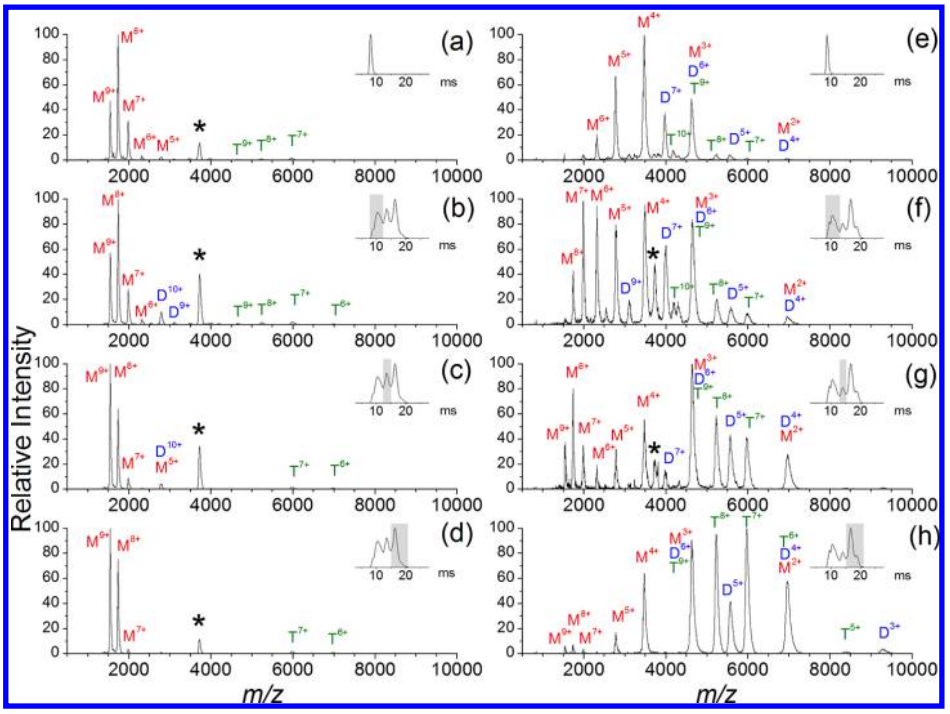

Figure 3. (a) CID spectrum of nativelike TTR tetramer +15 at a cone voltage of 30 V. (b–d) Extracted IM-CID spectra of the unfolded TTR tetramer +15 at a cone voltage of 117 V. (e) SID spectrum of nativelike TTR tetramer +15 at a cone voltage of 30 V. (f–h) Extracted IM-SID spectra of the unfolded TTR tetramer +15 at a cone voltage of 117 V. Drift time distributions are shown as insets in each spectrum. The drift time regions that were used for extraction of spectra are shaded in each inset. All CID spectra were acquired at acceleration voltages of 90 V, and all SID spectra were at 70 V. Identities of major peaks are labeled, and their charge states are indicated with superscripts (M, monomer; D, dimer; T, trimer; asterisk, remaining precursor).

the SID spectrum (Figure 2f). The distribution of doubly charged products is centered at a lower m/z with SID than with CID. In other words, the precursor dissociated into smaller charged clusters in a more symmetric manner in SID than in CID. Singly charged product ions $Cs(CsI)_y^+$ spanned from y = 1 up to y = 46 in the detectable range, some of which are complementary to the doubly charged products, and others could be formed by secondary dissociation. Certain products (noted with an asterisk in Figure 2e,f), such as $Cs(CsI)_{13}^+$ (m/z = 3510.4) and $Cs(CsI)_{37}^+$ (m/z = 9745.9), have abundance significantly higher than that of their adjacent peaks and do not follow a statistical distribution. These products are believed to have "magic numbers" of atoms and adopt a cubiclike structure, resulting in a high stability that has been explored in the literature.[8,35]

These results demonstrated the advantage of separating overlapping m/z species for less ambiguous interpretation of MS/MS spectra. Spectra of all the overlapping species of $Cs_n(CsI)_{23n}^{n+}$ were acquired in one single MS-IM-MS experiment. Subsequently, the spectra at a specific drift time are extracted and examined individually without interference from other species. In addition, the SID in our modified instrument provides alternative dissociation pathways not accessible in CID. It is interesting to note that highly charged products (z > 3) are almost absent in both CID and SID spectra for $Cs_n(CsI)_{23n}^{n+}$ (n = 3–5) precursors (data not shown for n > 3). This is possibly a result of discrimination in focusing due to the wide distribution of kinetic energies, but an alternative explanation is derived from a report that unstable alkali halide clusters with high charges from excess metal ions could be formed from aggregation of smaller stable "core" clusters.[37] Thus, we also speculate that CsI clusters with charges higher than +3 may not form large and highly charged product ions after activation because of prompt dissociation into smaller stable clusters. Interestingly, this observation is reminiscent of recent findings by Borysik et al. where detergent clusters with long chain length did not show stable intermediate products in CID.[38]

SID Spectra Are Sensitive to the Conformation of Protein Complexes. Transthyretin (TTR) forms a homotetramer under physiological conditions. Studies by Ruotolo et al. with IM[28] showed that the tetramer complex activated by elevated cone voltage in the ion source exhibited multiple distinct species with different conformations. Given the time scale of the instrument, these conformations have to be stable in the gas phase for on the order of milliseconds to be detected. On the basis of theoretical modeling results, they attributed the increase in drift times to partial unfolding of monomer subunits in the TTR tetramer (+15) upon in-source activation. However, there has not been direct experimental evidence from MS/MS in the literature to support the conclusions from theoretical modeling.

Representative CID/SID spectra for nativelike TTR tetramer (+15) under gentle source conditions are exhibited in Figure 3a,e. The +15 charge state of the tetramer was selected in this study because this tetramer precursor does not overlap with other smaller TTR oligomers in m/z. The same potential drop of 90 V from the exit of IM cell to the transfer TWIG was used for both CID and SID for direct comparison under minimum differences in voltage settings, although the effective acceleration in SID is only 70 V due to the use of 20 V acceleration to transfer the SID products downstream. Drift time distributions of the precursors are shown as insets in each spectrum and exhibit compact conformations indicative of

dx.doi.org/10.1021/ac300810u | Anal. Chem. 2012, 84, 6016–6023

nativelike structure. In the CID spectrum (Figure 3a) the most intense monomer product has a charge of +8, and the complementary trimer product with +7 can be clearly seen in the higher m/z region. Given an even distribution of the charge within the complex, each monomer should carry about 4 charges to satisfy a total charge of 15 in the tetramer. In contrast to dominant monomers with +8 charges in CID, monomer products of TTR with a charge of +4 are prevalent in the SID spectrum (Figure 3e), implying a more symmetric dissociation pathway in SID than in CID. The appearance of CID spectra does not change qualitatively up to 120 V except for a gradual decrease in the abundance of the remaining precursor. Under higher acceleration voltages, peptide fragments from the protein backbone emerge but the highly charged monomer products are still dominant in the spectra. SID spectra resemble CID spectra, with highly charged monomer products when the acceleration energy is around 30 V (at internal energies just above the dissociation threshold), but at higher voltages SID spectra feature predominantly low-charged monomers.[7] Several studies have provided some evidence that CID dissociation involves gradual unfolding of a monomeric subunit that takes a large portion of the charge from the precursor due to the large exposed surface area.[10,13] We hypothesized in our previous work[7] that the symmetric charge distribution among monomer products in SID is attributed to the fast, high energy deposition and absence of significant subunit unfolding during the SID process, which has recently been confirmed by SID-IM experiments.[16]

To better understand the unfolding intermediates reported by Ruotolo et al.,[28] MS/MS experiments under the same CID and SID acceleration voltages (90 and 70 V, respectively) as the nativelike precursors were performed at the same source cone voltage of 117 V where the multiple structures were detected (Figure 3b–d,f–h). Inserted drift time distributions in Figure 3 show distinct multiple conformations within the precursor population (same m/z, different conformations) that was isolated by the quadrupole after source activation. The variation in the relative abundances of the different conformations of the precursor is speculated to be a consequence of differences in the distributions of kinetic and internal energies/extent of dissociation after activation by CID or SID; note that the arrival time distributions shown here convolute the IM separation, the activation and dissociation steps, and the transfer time from the exit of IM cell to the TOF. The profile is sensitive to instrument voltage settings, and the spectra shown here were acquired under conditions that give a good signal for all major conformations. CID spectra of the three major ensembles of conformations at the cone voltage of 117 V are extracted and presented in the left column of Figure 3b–d. They all share the same typical CID dissociation pattern as the nativelike structure (Figure 3a), which involves ejection of highly charged monomers (+7 to +9) and complementary trimers (+8 to +6). A major difference between the unfolded structure and the nativelike structure is the survival yield of the tetramer precursor. In CID spectra, the nativelike precursor has the lowest relative intensity (Figure 3a–d). Among the CID spectra of cone-activated species, the survival yield of the tetramer precursor decreased at longer drift times. These observations can be rationalized by the hypothesis of a stepwise CID dissociation mechanism that involves subunit unfolding. The precursors at longer drift times are at later stages of unfolding after source activation, which result in higher efficiencies of subsequent monomer ejection in the CID process. Another minor difference among the CID spectra is the charge state distribution of the monomer products. It can be observed that higher charged monomers (+9) are more intense for precursors at longer drift times, which are speculated to be more unfolded. However, the overall pattern of CID spectra does not change significantly among the different conformations; highly charged, presumably partially unfolded monomers dominate all spectra.

The extracted SID spectra for the multiple TTR tetramers with different extents of unfolding are displayed in Figure 3f–h (drift time shown by the insets). Differences are obvious when comparing the different structures formed by source activation. For the structures at drift times longer than that of the nativelike conformation (Figure 3e), a remarkable amount of trimers and complementary highly charged monomers (+7 to +9) was observed in the SID spectra, indicating that the precursors at longer drift times are different from the nativelike fold. The +7 to +9 monomer products support the modeling study that one of the monomers in the complex had been partially unfolded in the complex as indicated by the high number of charges. As the protein unfolds, the structure of the complex becomes asymmetric, contributing to the asymmetric dissociation pattern observed in the SID spectra of source-unfolded precursor. The varying ratios of low m/z (monomers) and high m/z (mostly trimers) products in the SID spectra could result from alternations in the energetics of differentially unfolded species, which deserves further examination and is not the emphasis of this work. Although CID spectra have provided some evidence of the differences in the structures separated by IM, the results are not conclusive evidence of their conformations because unfolding is usually a prerequisite of dissociation in CID. In contrast, the SID results shown here are sensitive to the precursor conformation, e.g., contrast Figure 3e vs f–h.

SID Provides Insights into Different Subunit Packing in Conformers of a Decameric Protein Complex. Human serum amyloid P (SAP) is a glycoprotein whose oligomerization properties are highly dependent on solution conditions. SAP pentamer adopts a ring structure as shown by crystallography results,[39] and the pentamers can assemble into decamers in a face-to-face orientation. Each SAP pentamer has one face (A face) containing five α-helices and the other face (B face) accommodating five double-calcium binding sites.[40] Decamers formed from the A–A interface,[39] A–B interface,[41] and B–B interface[40] have all been reported. Additionally, conformations of the ligand[42] or the oligosaccharide chain[43] have been shown to affect the structure of the decamer. Mass spectrometry analysis of SAP has exhibited a suppression of decameric form in the presence of calcium which reflects its properties in vivo, and higher order of oligomerization under specific ligand conditions.[44] We present here the capability of IM-SID to differentiate conformers of SAP decamers under nativelike conditions in absence of physiological ligand.

A distinct bimodal drift time distribution can be observed for SAP decamer (100 μM/monomer) in 200 mM ammonium acetate sprayed under gentle source conditions, implying multiple gas-phase structures of the decamer (Figure 4a). Decamers at shorter drift times should have more compact structures than the ones at longer drift times. This difference in compactness of the decamer might possibly originate from different orientation of oligosaccharide chains at the interface, which has been shown as a factor affecting the thickness of the decamer.[43] The +35 charge state (m/z 7356) was selected with

dx.doi.org/10.1021/ac300810u | Anal. Chem. 2012, 84, 6016–6023

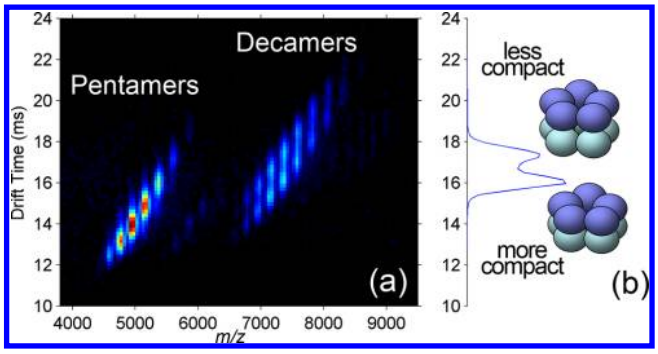

Figure 4. (a) Drift time vs m/z of SAP sprayed under gentle source conditions. A bimodal distribution in drift time can be clearly observed for the decamers. (b) Drift time distribution for the precursor (+35). The decamers at shorter drift times is likely to be more compact than the one at longer drift times as shown by the cartoon.

the quadrupole, the drift time distribution of which is shown in Figure 4b, for subsequent IM-CID and IM-SID experiments (Figure 5). The peaks broadened in drift time to different

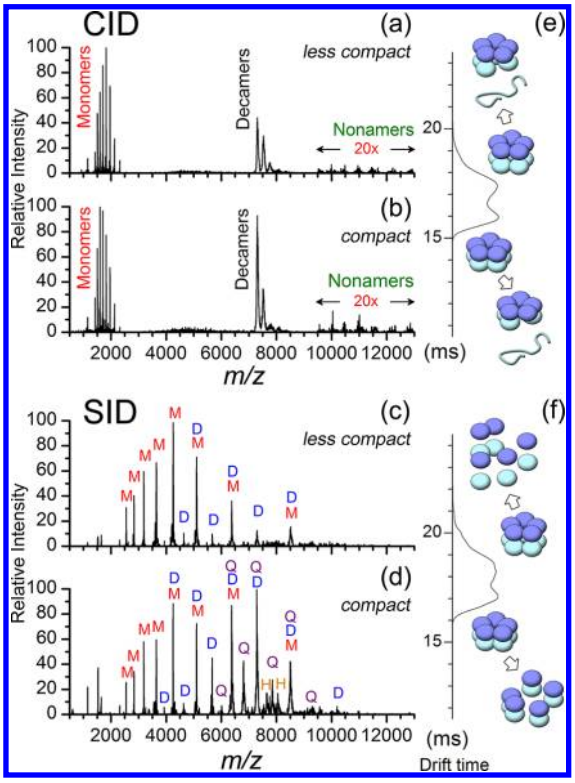

Figure 5. CID of the (a) less compact and (b) compact SAP decamer at 160 V. SID of the (c) less compact and (d) compact SAP decamer at 120 V. Major peaks are labeled in the spectra (M, monomer; D, dimer; Q, tetramer; H, hexamer). (e, f) Corresponding drift time distribution showing separation of CID/SID products from less compact and compact SAP decamers. Insets show schematics for plausible dissociation pathways.

extents probably due to alternations in energy distributions after CID/SID activation. The profile in the SID is slightly shifted to longer drift times by 1 ms compared with CID because of a longer trajectory the ions had to traverse in the transfer TWIG, which becomes more pronounced for large molecules with lower velocities. CID spectra at 160 V acceleration corresponding to different drift times are presented in Figure 5a,b and are qualitatively similar except for the noticeably lower precursor survival for the species of less compact structure. Again, no qualitative difference in the spectra other than the precursor survival yields is observed. Monomer products carrying charges from +11 to +18 were observed along with complementary nonamers. Within accessible acceleration voltages, no further qualitative differences in CID spectra are found, likely due to the fact that the proteins undergo the same unfolding pathway upon activation in CID (Figure 5e). However, differences can be clearly seen between the compact and less compact decamers for the SID spectra at 120 V (Figure 5c,d). The SID acceleration voltage shown here was chosen to yield sufficient products without too much excess energy to cause secondary dissociation of large subunit products. Other than the common monomer and dimer products in both of the SID spectra, tetramer and hexamer products are present in the SID spectrum of the compact decamers. It is interesting to note that with the exception of the monomer product, the exclusive products of the more compact decamers all have an even number of subunits. Furthermore, the relative abundance of the dimer products in the compact decamers is considerably higher than that in the less compact decamer.

We speculate that there are stronger interactions at the pentamer−pentamer interfaces in the more compact decamers than in the less compact decamers. At the same SID acceleration energy, dimer, tetramer, and hexamer products are better preserved for the compact precursor. To obtain these products, especially the hexamer, dissociation of the compact decamers in SID must occur at the dimer−dimer interface perpendicular to the pentameric ring, maintaining the interface between two rings in the products (Figure 5f). The different gas-phase structures are potentially physiologically relevant because SAP pentamers are known to have various configurations to be stacked into decamers under different conditions as mentioned earlier. The two distributions observed here might originate from differences in oligosaccharide chain interactions as supported by the different drift times and corresponding SID spectra of the precursors, because the solutions are free of physiological ligands for SAP. It is of great interest to pursue this study on decamer structures under different ligand binding conditions in the future.

CONCLUSION

A custom in-line SID device has been successfully incorporated into a modified commercial Q-IM-TOF instrument, allowing direct comparison of IM-CID and IM-SID under the same instrument conditions. The capability of separating complicated mixtures by IM and activating them by CID or SID in our modified instrument has exhibited advantages over conventional mass spectrometers. MS/MS of precursors that share the same m/z but differ in size or shape can be examined individually for identification at a millisecond time scale. This greatly reduces the complexity of MS/MS spectra and enhances the quality of interpretation. For large noncovalent protein complexes or for inorganic clusters, SID spectra provide different and potentially more informative data than CID spectra. For protein complexes in particular, SID spectra show distinct differences between different conformations of TTR tetramers, and SID spectra also reflect the differences in subunit packing in SAP decamers. It can be concluded that IM-SID holds great potential for structural analysis of protein complexes because it can reflect the differences in the

dx.doi.org/10.1021/ac300810u | Anal. Chem. 2012, 84, 6016−6023

quaternary structures of precursors. Future directions will include improvement of the current SID design to increase the transmission of the device especially for very large complexes in the mega Dalton mass range to better solve complicated but intriguing structural problems with high biological significance.

AUTHOR INFORMATION

Corresponding Author

*E-mail: vwysocki@email.arizona.edu.

Notes

The authors declare no competing financial interest.

ACKNOWLEDGMENTS

The authors acknowledge Kevin Giles from Waters Corporation for helpful discussions. We also thank Dr. Shai Dagan for helpful discussions during the preparation of the manuscript. We are grateful for financial support from the National Science Foundation (Grant 0923551 to V.H.W.) and the Science Foundation of Arizona (Graduate Research Fellowship for C.H.).

REFERENCES

(1) Heck, A. J. R. *Nat. Methods* **2008**, *5*, 927−933.
(2) Heuvel, R. H. H. v. d.; Heck, A. J. R. *Curr. Opin. Chem. Biol.* **2004**, *8*, 519−526.
(3) Hernández, H.; Robinson, C. *Nat. Protoc.* **2007**, *2*, 715−726.
(4) Sobott, F.; Robinson, C. V. *Principles of Mass Spectrometry Applied to Biomolecules*; John Wiley & Sons, Inc.: New York, 2006; pp 147−175.
(5) Jones, C. M.; Beardsley, R. L.; Galhena, A. S.; Dagan, S.; Cheng, G.; Wysocki, V. H. *J. Am. Chem. Soc.* **2006**, *128*, 15044−15045.
(6) Wysocki, V. H.; Joyce, K. E.; Jones, C. M.; Beardsley, R. L. *J. Am. Soc. Mass Spectrom.* **2008**, *19*, 190−208.
(7) Beardsley, R. L.; Jones, C. M.; Galhena, A. S.; Wysocki, V. H. *Anal. Chem.* **2009**, *81*, 1347−1356.
(8) Galhena, A. S.; Jones, C. M.; Wysocki, V. H. *Int. J. Mass Spectrom.* **2009**, *287*, 105−113.
(9) Jurchen, J. C.; Garcia, D. E.; Williams, E. R. *J. Am. Soc. Mass Spectrom.* **2004**, *15*, 1408−1415.
(10) Jurchen, J. C.; Williams, E. R. *J. Am. Chem. Soc.* **2003**, *125*, 2817−2826.
(11) Sinelnikov, I.; Kitova, E. N.; Klassen, J. S. *J. Am. Soc. Mass Spectrom.* **2007**, *18*, 617−631.
(12) Sciuto, S.; Liu, J.; Konermann, L. *J. Am. Soc. Mass Spectrom.* **2011**, *22*, 1679−1689.
(13) Benesch, J. L. P.; Aquilina, J. A.; Ruotolo, B. T.; Sobott, F.; Robinson, C. V. *Chem. Biol.* **2006**, *13*, 597−605.
(14) Wanasundara, S. N.; Thachuk, M. *J. Phys. Chem. B* **2009**, *113*, 3814−3821.
(15) Wanasundara, S. N.; Thachuk, M. *J. Phys. Chem. B* **2010**, *114*, 11646−11653.
(16) Zhou, M.; Dagan, S.; Wysocki, V. H. *Angew. Chem., Int. Ed.* **2012**, *51*, 4336−4339.
(17) Zhang, H.; Cui, W.; Wen, J.; Blankenship, R. E.; Gross, M. L. *Anal. Chem.* **2011**, *83*, 5598−5606.
(18) Blackwell, A. E.; Dodds, E. D.; Bandarian, V.; Wysocki, V. H. *Anal. Chem.* **2011**, *83*, 2862−2865.
(19) Bleiholder, C.; Dupuis, N. F.; Wyttenbach, T.; Bowers, M. T. *Nature Chem.* **2011**, *3*, 172−177.
(20) Kloniecki, M.; Jablonowska, A.; Poznanski, J.; Langridge, J.; Hughes, C.; Campuzano, I.; Giles, K.; Dadlez, M. *J. Mol. Biol.* **2011**, *407*, 110−124.
(21) Duijn, E. v.; Barendregt, A.; Synowsky, S.; Versluis, C.; Heck, A. J. R. *J. Am. Chem. Soc.* **2009**, *131*, 1452−1459.
(22) Uetrecht, C.; Barbu, I. M.; Shoemaker, G. K.; Duijn, E. v.; Heck, A. J. R. *Nature Chem.* **2011**, *3*, 126−132.
(23) Knapman, T. W.; Morton, V. L.; Stonehouse, N. J.; Stockley, P. G.; Ashcroft, A. E. *Rapid Commun. Mass Spectrom.* **2010**, *24*, 3033−3042.
(24) Hogan, C. J.; Ruotolo, B. T.; Robinson, C. V.; Fernandez de la Mora, J. *J. Phys. Chem. B* **2011**, *115*, 3614−3621.
(25) *Gel Filtration Principles and Methods*; GE Healthcare: Piscataway, NJ, 2010.
(26) Rambaldi, D.; Reschiglian, P.; Zattoni, A. *Anal. Bioanal. Chem.* **2011**, *399*, 1439−1447.
(27) Freeke, J.; Bush, M. F.; Robinson, C. V.; Ruotolo, B. T. *Chem. Phys. Lett.* **2012**, *524*, 1−9.
(28) Ruotolo, B. T.; Hyung, S.-J.; Robinson, P. M.; Giles, K.; Bateman, R. H.; Robinson, C. V. *Angew. Chem., Int. Ed.* **2007**, *46*, 8001−8004.
(29) Freeke, J.; Robinson, C. V.; Ruotolo, B. T. *Int. J. Mass Spectrom.* **2010**, *298*, 91−98.
(30) Hall, Z.; Politis, A.; Bush, M. F.; Smith, L. J.; Robinson, C. V. *J. Am. Chem. Soc.* **2012**, *134*, 3429−3438.
(31) Giles, K.; Williams, J. P.; Campuzano, I. *Rapid Commun. Mass Spectrom.* **2011**, *25*, 1559−1566.
(32) Zhong, Y.; Hyung, S.-J.; Ruotolo, B. T. *Analyst* **2011**, *136*, 3534−3541.
(33) Galhena, A. S.; Dagan, S.; Jones, C. M.; Beardsley, R. L.; Wysocki, V. H. *Anal. Chem.* **2008**, *80*, 1425−1426.
(34) Hill, H. H.; Hill, C. H.; Asbury, G. R.; Wu, C.; Matz, L. M.; Ichiye, T. *Int. J. Mass Spectrom.* **2002**, *219*, 23−37.
(35) Twu, Y. J.; Conover, C. W. S.; Yang, Y. A.; Bloomfield, L. A. *Phys. Rev. B* **1990**, *42*, 5306.
(36) Beck, R. D.; John, P. S.; Homer, M. L.; Whetten, R. L. *Science* **1991**, *253*, 879−883.
(37) Sugai, T.; Shinohara, H. *Chem. Phys. Lett.* **1997**, *281*, 57−62.
(38) Borysik, A. J.; Robinson, C. V. *Langmuir* **2012**, *28*, 7160−7167.
(39) Emsley, J.; White, H. E.; O'Hara, B. P.; Oliva, G.; Srinivasan, N.; Tickle, I. J.; Blundell, T. L.; Pepys, M. B.; Wood, S. P. *Nature* **1994**, *367*, 338−345.
(40) Hohenester, E.; Hutchinson, W. L.; Pepys, M. B.; Wood, S. P. *J. Mol. Biol.* **1997**, *269*, 570−578.
(41) Thompson, D.; Pepys, M. B.; Tickle, I.; Wood, S. *J. Mol. Biol.* **2002**, *320*, 1081−1086.
(42) Ho, J. G. S.; Kitov, P. I.; Paszkiewicz, E.; Sadowska, J.; Bundle, D. R.; Ng, K. K.-S. *J. Biol. Chem.* **2005**, *280*, 31999−32008.
(43) Ashton, A. W.; Boehm, M. K.; Gallimore, J. R.; Pepys, M. B.; Perkins, S. J. *J. Mol. Biol.* **1997**, *272*, 408−422.
(44) Aquilina, J. A.; Robinson, C. V. *Biochem. J.* **2003**, *375*, 323−328.